Human Molecular Genetics, 2014, Vol. 23, No. 9 **2447–2458**
doi:10.1093/hmg/ddt640
Advance Access published on December 18, 2013

Mice with an isoform-ablating *Mecp2* exon 1 mutation recapitulate the neurologic deficits of Rett syndrome

Dag H. Yasui[1,*], Michael L. Gonzales[2], Justin O. Aflatooni[1], Florence K. Crary[1], Daniel J. Hu[3], Bryant J. Gavino[3], Mari S. Golub[3,4], John B. Vincent[5], N. Carolyn Schanen[6,7], Carl O. Olson[8], Mojgan Rastegar[8] and Janine M. Lasalle[1,9,10]

[1]Department of Medical Microbiology and Immunology, UC Davis, Davis, CA, USA [2]Fluidigm, South San Francisco, CA, USA [3]UC Davis Mouse Biology Program, Davis, CA, USA [4]UC Davis California Regional Primate Research Center, Davis, CA, USA [5]The Campbell Family Brain Research Institute, Centre for Addiction and Mental Health, Toronto, ON, Canada [6]Department of Biological Sciences, University of Delaware, Newark, DE, USA [7]Nemours Biomedical Research Institute, A.I. DuPont Hospital, Wilmington, DE, USA [8]Department of Biochemistry and Medical Genetics, University of Manitoba, Winnipeg, MB, Canada [9]UC Davis Genome Center, Davis, CA, USA [10]UC Davis MIND Institute, Sacramento, CA, USA

Received September 20, 2013; Revised November 21, 2013; Accepted December 12, 2013

Mutations in *MECP2* cause the neurodevelopmental disorder Rett syndrome (RTT OMIM 312750). Alternative inclusion of *MECP2/Mecp2* exon 1 with exons 3 and 4 encodes MeCP2-e1 or MeCP2-e2 protein isoforms with unique amino termini. While most *MECP2* mutations are located in exons 3 and 4 thus affecting both isoforms, *MECP2* exon 1 mutations but not exon 2 mutations have been identified in RTT patients, suggesting that MeCP2-e1 deficiency is sufficient to cause RTT. As expected, genetic deletion of *Mecp2* exons 3 and/or 4 recapitulates RTT-like neurologic defects in mice. However, *Mecp2* exon 2 knockout mice have normal neurologic function. Here, a naturally occurring *MECP2* exon 1 mutation is recapitulated in a mouse model by genetic engineering. A point mutation in the translational start codon of *Mecp2* exon 1, transmitted through the germline, ablates MeCP2-e1 translation while preserving MeCP2-e2 production in mouse brain. The resulting MeCP2-e1 deficient mice developed forelimb stereotypy, hindlimb clasping, excessive grooming and hypo-activity prior to death between 7 and 31 weeks. MeCP2-e1 deficient mice also exhibited abnormal anxiety, sociability and ambulation. Despite MeCP2-e1 and MeCP2-e2 sharing, 96% amino acid identity, differences were identified. A fraction of phosphorylated MeCP2-e1 differed from the bulk of MeCP2 in subnuclear localization and co-factor interaction. Furthermore, MeCP2-e1 exhibited enhanced stability compared with MeCP2-e2 in neurons. Therefore, MeCP2-e1 deficient mice implicate MeCP2-e1 as the sole contributor to RTT with non-redundant functions.

INTRODUCTION

Although the majority of Rett syndrome cases are caused by *MECP2* mutations (1), the molecular mechanisms underlying this neurological disorder are not fully understood. Originally, *MECP2* encoding the methyl CpG-binding protein MeCP2 was believed to consist of three exons (2). However, a fourth upstream *MECP2*/*Mecp2* coding exon was later identified that due to alternative splicing produces an MeCP2 protein isoform with a higher brain abundance than the initially described isoform (3–5) (Supplementary Material, Fig. S1). This novel isoform was subsequently designated MeCP2-e1 while the original isoform was designated MeCP2-e2 to reflect the alternate inclusion of coding exon 2. Thus, the human MeCP2 isoforms differ by only the unique 21 or 9 amino acids encoded by spliced exons 1 or 2 containing messenger RNA, respectively (4) (Supplementary Material, Fig. S1B). Although up to 95% of RTT-associated mutations occur in *MECP2* exons 3 and 4 encoded amino acids common to both isoforms, genetic screening has identified *MECP2* exon 1 mutations in up to 1% of RTT patients (6–8). But no *MECP2* exon 2 mutations have been identified in patients, suggesting that MeCP2-e1 deficiency alone contributes to

*To whom correspondence should be addressed at: Medical Microbiology and Immunology, UC Davis School of Medicine, One Shields Avenue, Davis, CA 95616, USA. Tel: +1 5307547906; fax: +1 5307528692; Email: dhyasui@ucdavis.edu

neurologic symptoms. As expected, *Mecp2* null alleles which lead to ablation of both MeCP2 isoforms generally recapitulate RTT-like symptoms in mouse models (9–11). However, genetic deletion of *Mecp2* exon 2 resulting in loss of only MeCP2-e2 expression is without significant neurologic symptoms, suggesting that this MeCP2 isoform does not have an essential function in the nervous system (12).

Therefore, to determine the specific relationship between MeCP2-e1 and RTT, MeCP2-e1 deficient mice were genetically engineered and assayed for symptoms common to those observed in Rett patients. MeCP2-e1 deficient mice were modeled on an orthologous *MECP2* exon 1 translational start site mutation identified in patients with classic RTT symptoms (8,13). Previous studies performed in RTT patient cell lines bearing this *MECP2* mutation predict that only MeCP2-e1 and not MeCP2-e2 will be ablated in this mouse model (13).

RESULTS

Generation of MeCP2-e1 deficient mice

While *Mecp2* whole exon deletion mice display RTT-like symptoms (9,10,14), these large genetic deletions only rarely occur in human RTT patients (mecp2.chw.edu.au). To test the hypothesis that MeCP2-e1 is the major contributor to RTT, we engineered a point mutation in the *Mecp2* exon 1 (*Mecp2-e1*) translational start site based on an orthologous RTT causing *MECP2* exon 1 mutation (8). This *Mecp2-e1* mutation construct was introduced into C57BL/6N embryos and propagated through the germline (Fig. 1). Chimeric founder males carrying the transgene were mated with wild-type (WT) C57BL/6N females to produce *Mecp2-e1*$^{+/-}$ heterozygous females. *Mecp2-e1*$^{+/-}$ females were then mated with WT C57BL/6N males producing pups of the four possible genotypes (*Mecp2-e1*$^{+/+}$, *Mecp2-e1*$^{-/+}$, *Mecp2-e1*$^{+/y}$, *Mecp2-e1*$^{-/y}$) at the expected frequencies, suggesting that embryonic development was not compromised. At birth, *Mecp2-e1*$^{-/y}$ pups were indistinguishable from WT *Mecp2-e1*$^{+/y}$ male littermates. However, by 6 weeks post-natal, *Mecp2-e1*$^{-/y}$ males began to exhibit characteristic neurologic symptoms, determined using a scoring system similar to one previously described for *Mecp2*$^{tm1.1Bird/J}$ mice (9) (Fig. 2A). Levels of grooming, ambulation, the presence of skin sores and abdomen size were scored along with specific responses to tail suspension including hind limb clasping, forelimb 'washing' and flailing motions (Supplementary Material, SV1). A significant contributor to disease were symptoms of stereotypic over grooming in *Mecp2-e1*$^{-/y}$ males which were absent in control littermates. Specifically, *Mecp2-e1*$^{-/y}$ males developed hair loss and eventually skin loss on the flanks, chest and tail region (Supplementary Material, SV2). Disease symptoms progressed with age in mice until premature death between 7 and 31 weeks (Fig. 2B). *Mecp2-e1*$^{-/y}$ males also exhibited possible seizure activity (Supplementary Material, SV3). In contrast, *Mecp2-e1*$^{-/+}$ heterozygous female mice exhibited relatively mild symptoms with delayed hind limb clasping (Supplementary Material, Fig. S2) (Supplementary Material, SV4).

As mice lacking both isoforms of MeCP2 (*Mecp2* null) are significantly smaller and lighter than control littermates (9,10), *Mecp2-e1*$^{-/y}$ and *Mecp2-e1*$^{+/y}$ mice were carefully weighed and measured. Surprisingly, there were no significant weight, body length or body mass index differences between either the *Mecp2-e1*$^{-/y}$ and *Mecp2-e1*$^{+/y}$ genotypes (Supplementary

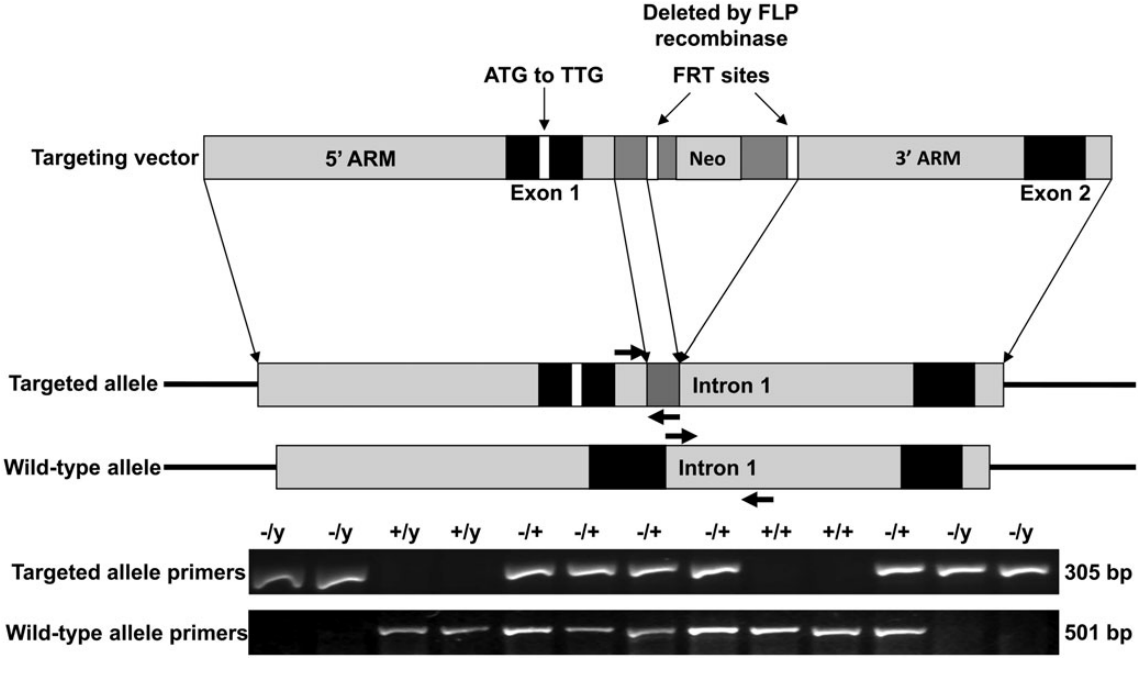

Figure 1. Targeting strategy for MeCP2-e1-specific germline ablation. Site directed mutagenesis was used to alter the *exon 1* translational start site ATG to TTG in the *Mecp2* locus excised from a genomic BAC clone. A neomycin resistance gene (NEO) flanked by flippase recognition target sites (FRT) was inserted into exon 1 to produce the targeting vector (top) which was then electroporated in C57BL/6N ES cells for homologous recombination. ES cells incorporating the targeting vector were selected for neomycin resistance then the NEO cassette was excised by expressing flippase, producing the mutant allele (middle). PCR primers detecting the mutant and WT *Mecp2* alleles are shown as colored arrows. Genotyping PCR was performed from DNA obtained from tail snips.

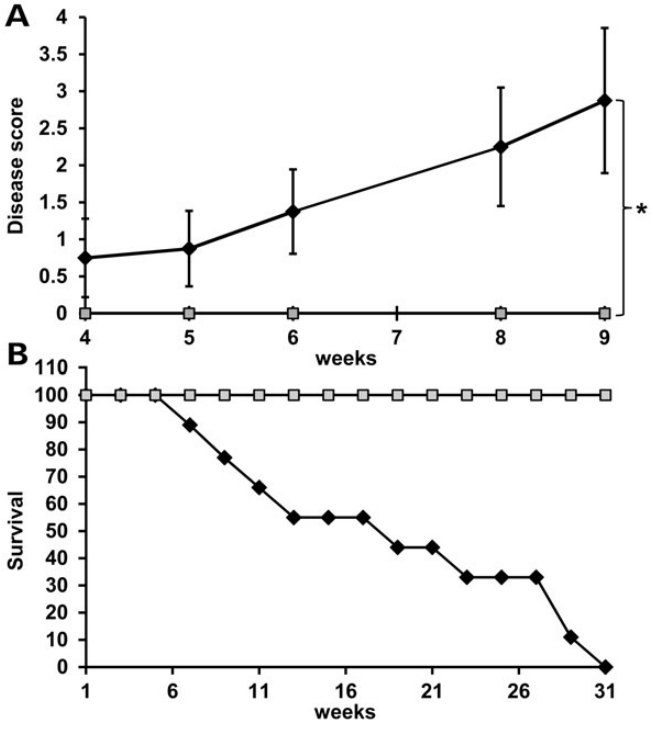

Figure 2. Mice with MeCP2-e1 isoform ablation exhibit neurologic disease and reduced lifespan. (**A**). Male *Mecp2-e1*$^{-/y}$ mice ($n = 8$) (black line) were scored along with control *Mecp2-e1*$^{+/y}$ male littermates ($n = 6$) (gray line) at weekly intervals for disease symptoms including matted fur, reduced ambulation, open skin sores, abnormally large abdomen along with hindlimb clasping, forelimb 'washing' and lack of body curling in response to tail suspension. Thus, the most diseased mice score '7' while completely healthy mice score '0'. Error bars correspond to standard error of the mean (SEM). $^*P = 0.0197$ by independent sample, two-tailed *t*-test. (**B**). Survival curve of *Mecp2-e1*$^{-/y}$ MeCP2-e1 deficient (black line) and WT control male littermate mice (gray line). $n = 11$ for *Mecp2-e1*$^{-/y}$ males and $n = 9$ for WT *Mecp2-e1*$^{+/y}$ control males.

Material, Table S1) or the *Mecp2-e1*$^{-/+}$ and *Mecp2-e1*$^{+/+}$ genotypes (data not shown).

MeCP2-e1 deficient mice have neurological deficits

As previous mouse models of RTT show behavioral abnormalities (9,10,14,15), *Mecp2-e1*$^{-/y}$ mice were subjected to tests of anxiety and sociability. In the elevated plus maze assay, *Mecp2-e1*$^{-/y}$ mice spent significantly more time in the open arms, indicative of reduced anxiety compared with control *Mecp2-e1*$^{+/y}$ littermates (Fig. 3A). To control for mobility in the EPM assay, center zone entries, time spent in the closed arms and walking speed in closed arms was recorded and found to be similar for both genotypes (Supplementary Material, Table S2). In addition, *Mecp2-e1*$^{-/y}$ mice spent significantly less time interacting with a test mouse in the three-chamber assay, indicating reduced sociability compared with WT *Mecp2-e1*$^{+/y}$ littermate controls (Fig. 3B). These results were not due to differences in activity as center chamber entries and entries of the mice into the area around the empty cage were not significantly different between *Mecp2-e1*$^{-/y}$ and control *Mecp2-e1*$^{+/y}$ mice (Supplementary Material, Table S2). As ambulatory defects are one of the most consistent symptoms of RTT, *Mecp2-e1*$^{-/y}$ mice were tested for gait abnormalities by tread scan analysis. *Mecp2-e1*$^{-/y}$ deficient mice had a slower running pace (Fig. 3C) and reduced variability in rear paw placement distance compared with control littermates (Fig. 3D) reminiscent of motor deficits observed in previous mouse models (9,10) and RTT (16).

To further examine the potential mechanisms underlying these defects, nuclear size was assayed in *Mecp2-e1*$^{-/y}$, and *Mecp2-e1*$^{+/y}$ hippocampal neurons (Supplementary Material, Fig. S3). *Mecp2-e1*$^{-/y}$ neurons had significantly smaller nuclei than control *Mecp2-e1*$^{+/y}$ littermates as expected from previous studies (9,10).

Confirmation of MeCP2-e1 ablation by immunofluorescence

To confirm the ablation of MeCP2-e1 protein in *Mecp2-e1* targeted mice and identify potential functional differences between the isoforms, immunofluorescence (IF) analysis was performed in *Mecp2-e1*$^{+/y}$ and *Mecp2-e1*$^{-/y}$ brain sections using an antibody (MeCP2-e1 JL) to the conserved N-terminus of MeCP2-e1 (Supplementary Material, Fig. S1). IF staining revealed that MeCP2-e1 JL staining was undetectable in all *Mecp2-e1*$^{-/y}$ brain regions including adult hippocampus, suggesting that *Mecp2-e1*$^{-/y}$ mice are truly deficient in MeCP2-e1 (Fig. 4A). However, in control *Mecp2-e1*$^{+/y}$ neurons, the MeCP2-e1 JL staining pattern was unexpectedly found to be predominately nucleoplasmic in distribution upon higher magnification (Fig. 4A, Supplementary Material, Figs. S4 and S5).

To confirm the absence of MeCP2-e1 in *Mecp2-e1*$^{-/y}$ brain with additional antibodies, IF was performed with two MeCP2-e1-specific antibodies designated MeCP2-e1 MR and MeCP2-e1 CS generated to overlapping but non-identical N-terminal peptide epitopes of MeCP2-e1 (Supplementary Material, Fig. S1B) (5). While both additional antibodies confirm the absence of MeCP2-e1 staining in *Mecp2-e1*$^{-/y}$ brain initially observed with the MeCP2-e1 JL antibody, the staining patterns that they produce show predominant MeCP2-e1 localization to chromocenters in control brain respectively (Supplementary Material, Figs S6 and S7) consistent with previous reports both *in vivo* (5) and *in vitro* (17–19).

Previous analysis of post-translational modifications demonstrated that MeCP2-e1 undergoes phosphorylation at serine 30 (pS30) (20) a site which was exclusively within the epitope for the MeCP2-e1 JL antibody. We therefore hypothesized that the MeCP2-e1 JL antibody was sensitive to MeCP2-e1 pS30, localized to heterochromatic chromocenters while the insensitive MeCP2-e1 CS and MeCP2-e1 MR antibodies detect total MeCP2-e1. (Supplementary Material, Fig. 1B). To directly investigate this hypothesis, IF staining patterns were compared with the original MeCP2-e1 JL antibody and the well characterized MeCP2-e1 MR antibody (5). These results show that MeCP2-e1 JL antibody detects MeCP2-e1 in the nucleoplasm while the MeCP2-e1 MR antibody detects both chromocenter and nucleoplasmic MeCP2-e1 (Supplementary Material, Fig. S8). To further investigate the sensitivity of the MeCP2-e1 JL antibody to pS30 of MeCP2-e1, peptides with and without pS30 were used as competitive inhibitors in IF, and these analyses showed the specificity of the MeCP2-e1 JL antibody to the non-phosphorylated N-terminus of MeCP2-e1 localized in the nucleoplasm (Supplementary Material, Fig. S9).

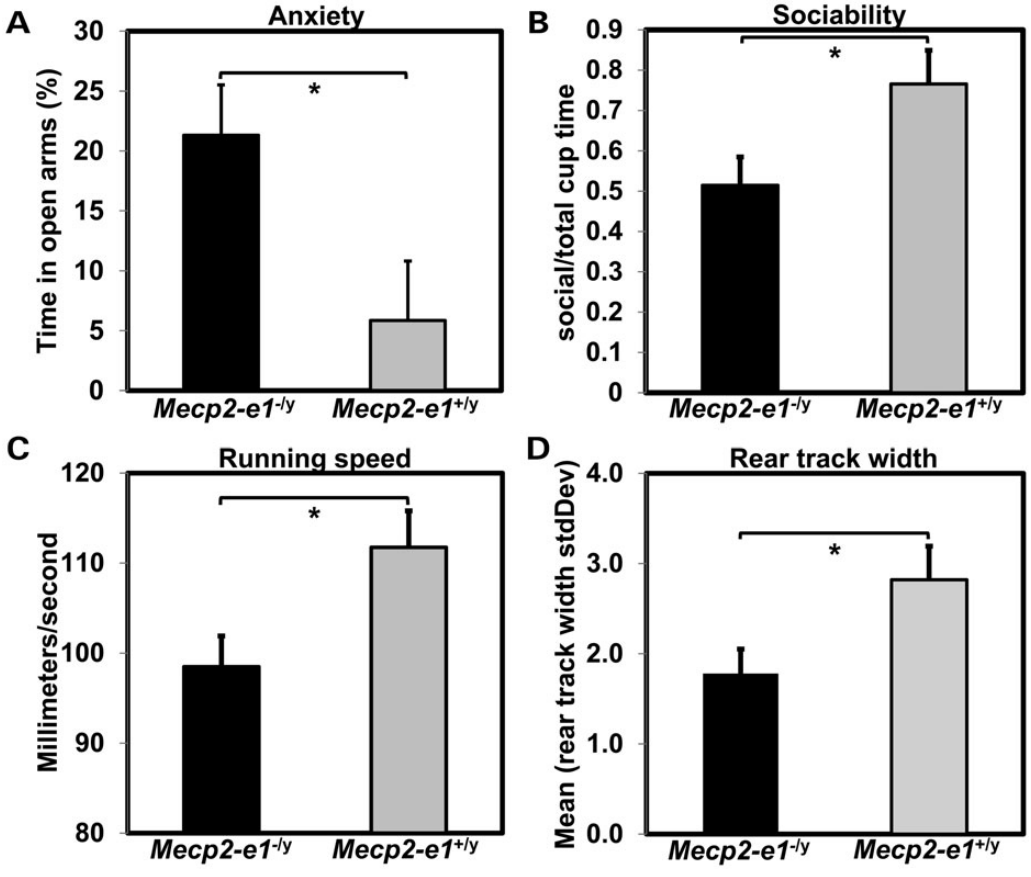

Figure 3. *Mecp2-e1*$^{-/y}$ mice exhibit behavioral abnormalities. (**A**). Anxiety measured in the elevated and maze (EPM) showed increased time in the open arms and thus reduced anxiety in *Mecp2-e1*$^{-/y}$ male mice ($P = 0.03$*). (**B**) Sociability measured in the three-chamber assay revealed a significant reduction in the percent time *Mecp2-e1*$^{-/y}$ mice spent near a cage containing a mouse relative to the total time spent near an occupied or an empty cage ($P = 0.048$*). (**C**). TreadScan analysis using a transparent treadmill belt combined with a high-speed video capture to measure instantaneous running speed and foot placement found that *Mecp2-e1*$^{-/y}$ male mice were significantly slower compared with WT controls ($P = 0.03$*). (**D**). TreadScan analysis revealed significantly reduced standard deviation in the rear track width distance between rear foot stance in *Mecp2-e1*$^{-/y}$ mice compared with WT controls ($P = 0.042$*). Error bars correspond to SEM. Genotype group comparisons were performed using least squares ANOVA. $n = 7$ *Mecp2-e1*$^{-/y}$ male mice, $n = 5$ WT *MeCP2-e1*$^{+/y}$ male littermate controls.

MeCP2-e2 levels and distribution were also assayed in parallel in brain by IF using a specific antibody (Supplementary Material, Fig. S1B) on brain sections from *Mecp2-e1*$^{-/y}$ and *Mecp2-e1*$^{+/y}$ littermates. As expected, MeCP2-e2 distribution appeared to be largely within the heterochromatic chromocenters (21,22) (Fig. 4B, Supplementary Material, S9). However, the overall MeCP2-e2 signal level appears elevated in *Mecp2-e1*$^{-/y}$ hippocampal neurons compared with *Mecp2-e1*$^{+/y}$ neurons (Fig. 4B).

Confirmation of MeCP2-e1 ablation by western blot

Western blot analysis was performed on brain protein extracts to independently verify the ablation of MeCP2-e1 and apparent elevation of MeCP2-e2 in *Mecp2-e1*$^{-/y}$ brain as shown by IF in Figure 4B. Probing of blots with MeCP2-e1 CS antibody from whole mouse brain extracts revealed barely detectable MeCP2-e1 levels in *Mecp2-e1*$^{-/y}$ brains compared with control *Mecp2-e1*$^{+/y}$ brain extracts (Fig. 5A and Supplementary Material, Fig. S10A). As the MeCP2-e1 CS antibody targets unmodified amino acids, it should recognize all forms of MeCP2-e1 in western blot analysis. These results are supported by western blot analysis of blood cells from Rett patients with orthologous *MECP2 exon 1* mutations that also reveal the absence of MeCP2-e1 (Supplementary Material, Fig. S10C). These results indicate that the naturally occurring *MECP2-e1* mutation as well as the *Mecp2-e1* engineered mutation functions as a null allele *in vivo*. Simultaneous probing of duplicate western blots showed an approximate 2-fold increase of MeCP2-e2 in *MeCP2-e1*$^{-/y}$ brain compared with control WT littermate brain (Fig. 5B), consistent with the IF images shown in Figure 4B. In light of the ablation of MeCP2-e1 and significant elevation of MeCP2-e2 in *Mecp2-e1*$^{-/y}$ brains, further western blot analysis was performed to determine the combined levels of both MeCP2 isoforms in brain, using a C-terminal antibody to total MeCP2. Interestingly, in spite of upregulated MeCP2-e2 levels in *Mecp2-e1*$^{-/y}$ brain, total MeCP2 levels were significantly reduced to ~50% of WT levels in *Mecp2-e1*$^{-/y}$ brains overall as shown by western (Fig. 5C).

MeCP2-e1 associates with components of the nuclear matrix

The elevated levels of MeCP2-e2 in *Mecp2-e1*$^{-/y}$ brain and the differential localization of non-pS30 and Mecp2-e1 pS30 in neurons both suggest that a sub-fraction of MeCP2-e1 has a unique function

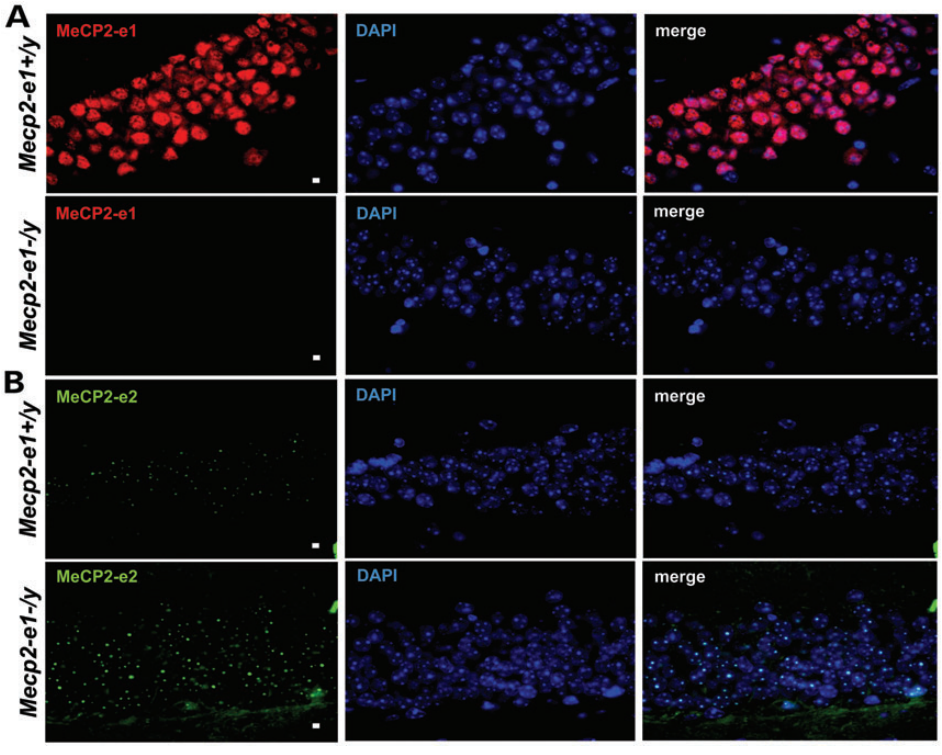

Figure 4. MeCP2-e1 is ablated in *Mecp2-e1*$^{-/y}$ mouse brain, while MeCP2-e2 levels are elevated as shown by IF. (**A**). IF detection of MeCP2-e1 in mouse hippocampus using a MeCP2-e1 JL specific antibody in adult *Mecp2-e1*$^{-/y}$ mutant and *Mecp2-e1*$^{+/y}$ control brain sections. Alexa 594-tagged (red) secondary antibodies were used to visualize the distribution of MeCP2-e1 in the nucleus. Higher magnification images are shown in Supplementary Material, Figure S1. (**B**). IF detection of MeCP2-e2 in mouse hippocampus using an MeCP2-e2 antibody with Alexa 488 (green) conjugated secondary in *Mecp2-e1*$^{-/y}$ and WT *Mecp2-e1*$^{+/y}$ control hippocampal sections. DAPI staining as shown in blue reveals the location of the nucleus in all panels. The scale bar represents 5 microns.

that cannot be replaced by MeCP2-e2. To further investigate the novel distribution of non-pS30 MeCP2-e1 outside of chromocenters, MeCP2-e1 associated co-factors were identified by immunoprecipitation (co-immuno-precipitation, co-IP) and mass spectrometric analysis (Fig. 6A). Interestingly, in two independent experiments, the nuclear matrix factors SFPQ (23) and Matrin 3 (24) were identified among the proteins that co-purified with MeCP2-e1 in neuronal nuclei in addition to the previously described associated co-factor YB-1 (Fig. 6B). The nuclear matrix is an insoluble structure (25) that organizes the genome into a series of non-random chromatin loops (26) that has been shown to regulate RNA stability, splicing, replication (24,27) and transcription (28). To determine the specificity of nuclear matrix factor co-purification with non-pS30 MeCP2-e1, the MeCP2-e1 JL antibody was tested for non-specific immunopurification of nuclear matrix factors from brain extracts lacking either MeCP2-e1 or MeCP2-e2 isoforms (Supplementary Material, Fig. S11). Neither the MeCP2-e1 JL antibody or an antibody recognizing both MeCP2 isoforms precipitated significant amounts of any protein in the absence of MeCP2, thereby providing a valuable negative control for these results.

In vivo association of MeCP2-e1 with Matrin 3 and SFPQ was assayed by IF analysis (Fig. 7). Co-staining with antibodies to SFPQ and MeCP2-e1 revealed that these factors largely co-localize in brain neuronal nuclei (Fig. 7A). Similarly, Matrin 3 and MeCP2-e1 IF signals exhibited a high degree of overlap suggesting molecular association in neuronal nuclei (Fig. 7B). As a positive control, IF analysis was performed using antibodies to the nuclear matrix factor SFPQ and YB-1 a factor previously shown to associate with MeCP2 (29). As expected, YB-1 signals overlapped with SFPQ signals on the nuclear matrix (Fig. 7C). Hence, these YB-1 results validate the interaction with and co-localization of nucleoplasmic MeCP2-e1 with SFPQ (Fig. 7A) and Matrin 3 (Fig. 7B). Additionally, molecular association of SFPQ, SFRS1 and Matrin 3 with MeCP2-e1 in brain was independently confirmed by co-IP and western blot analysis (Supplementary Material, Fig. S12). Therefore, association with nuclear matrix factors distinguishes MeCP2-e1 function from the hypothesized role of MeCP2 as a transcriptional repressor localized to heterochromatin in chromocenters (21,30).

MeCP2-e1 has greater stability in neurons than MeCP2-e2

MeCP2 isoform stability analysis was performed in human SHSY-5Y neurons in order to explore further functional differences between MeCP2-e1 and MeCP2-e2 protein isoforms. For these studies, the stability of MeCP2-Flag epitope-tagged proteins was monitored over time after shutdown of protein expression (Fig. 8). Western analysis reveals the gradual loss of both MeCP2-Flag isoforms over time (Fig. 8A), However, MeCP2-e2 levels were reduced to 20% of original levels by 24 h, while MeCP2-e1 levels diminished more slowly and only reached 20% of original levels after 48 h (Fig. 8B). These results suggest that differential MeCP2 isoform stability may

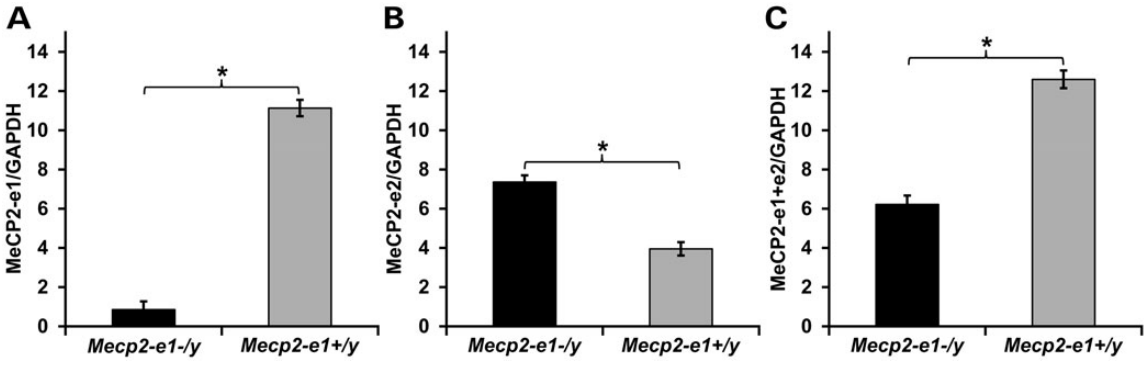

Figure 5. Western blot analysis of brain MeCP2 isoform levels confirms loss of MeCP2-e1 and overexpression of MeCP2-e2. Total brain proteins from *Mecp2-e1*$^{-/y}$ and *Mecp2-e1*$^{+/y}$ control males were probed with an MeCP2-e1 CS specific antibody in (**A**) which shows barely detectable MeCP2-e1 levels in *Mecp2-e1*$^{-/y}$ brain and significantly higher levels in WT control male brain ($P = 0.0019$). (**B**) An anti-MeCP2-e2-specific antibody revealed significant elevation of this isoform ($P = 0.0005$) in *Mecp2-e1*$^{-/y}$ brain compared with WT (*Mecp2-e1*$^{+/y}$) controls. (**C**) To determine the combined levels of MeCP2-e1 and MeCP2-e2 isoforms, an antibody recognizing a common epitope (Fig. S1) revealed an ~2-fold reduction of total MeCP2 in *Mecp2-e1*$^{-/y}$ deficient brain by western analysis ($P = 0.01$). Bar graphs depict average signal intensity from NIH Image J analysis of western blots with error bars corresponding to SEM. Three to four individual mouse brain protein extracts per genotype were analyzed.

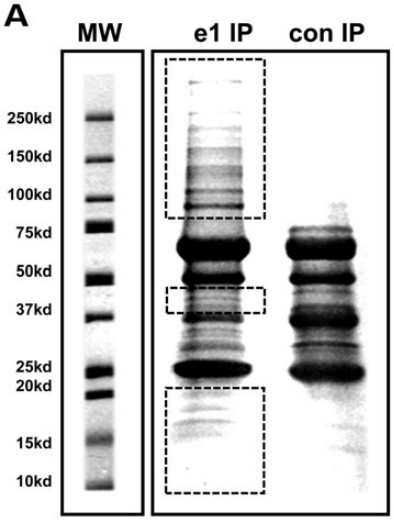

B peptides identified by Mass Spectrometry

Gene	Protein name	Sequence coverage (replicate)	Cellular location and function
MATR3	Matrin 3, MGC9105, KIAA0723	17%, 12.9%	Nuclear matrix, splicing, retention of defective RNA, transcriptional regulation
SFPQ	SFPQ, Matrin 4, PSF POMP-100, splicing Factor proline/glutamine rich, homologous DNA pairing protein	24.2% 8.6%	Nuclear matrix, RNA binding and splicing, developmentally regulated in neurons, transcriptional regulation, binds Sin3a
SFRS1	Splicing factor arginine/serine rich, ASF1	21.3% 11.6%	Nuclear and cytoplasmic, regulates alternative splicing, prevents exon skipping
YB-1	YBX-1, NSEP1, CBF-A	52%	Nucleus, RNA/DNA binding, splicing, transcriptional regulation,

Figure 6. MeCP2-e1-associated protein identification by mass spectrometric analysis. (**A**) SDS–PAGE resolved MeCP2 protein complexes were purified from human SH-SY5Y neurons using MeCP2-e1 JL antibody. Proteins not co-migrating with IP antibody heavy and light chains (red boxes) were selected for proteomic analysis. A control antibody IP with pre-immune IgY is shown on the right. Molecular weight standards are shown for estimation of molecular size in kilo Daltons. (**B**) Selected MeCP2-e1 associated factors identified by mass spectrometric analysis. Factors were listed based on significant amino acids identified (sequence coverage) in two separate experiments (replicate). YB-1, which was previously found to be associated with MeCP2, is shown as a control.

contribute to higher levels of MeCP2-e1 versus MeCP2-e2 in brain.

DISCUSSION

These results from the first MeCP2-e1 deficient mouse model of RTT provide direct experimental evidence that MeCP2-e1 is an essential isoform for normal neurologic function with unique activities that are not fully compensated for by MeCP2-e2. Our results are consistent with several previous studies that have suggested the critical role of MeCP2-e1 in the pathogenesis of RTT (4,8,13). First, the novel MeCP2-e1 isoform was found to be the predominant MeCP2 isoform in the mammalian central nervous system, with a higher translation efficiency of the *Mecp2* exon 1 start site compared with the exon 2 start site (3). Second, the presence of *MECP2* exon 1 but not exon 2 mutations in patients with classic RTT suggest that the MeCP2-e1 isoform is critical for normal neurologic function (4,8,13). Third, a mouse model with a deletion in *Mecp2* exon 2 failed to recapitulate neurologic symptoms characteristic of RTT (12). Fourth, it has been estimated that MeCP2-e1 is up to 10 times more abundant than MeCP2-e2 in mouse brain (3). Finally, the apparent absence of MeCP2-e1 in cells lines with orthologous *MECP2-e1* mutations from classic RTT patients suggest that MeCP2-e1 is essential for normal brain function (13).

The results presented here accurately recreate RTT in mice and are thus highly relevant to the pathology of the disease. While most previous mouse models of Rett syndrome are deletions of one or more whole *Mecp2* exons, the vast majority of *MECP2* mutations occurring in RTT are actually point

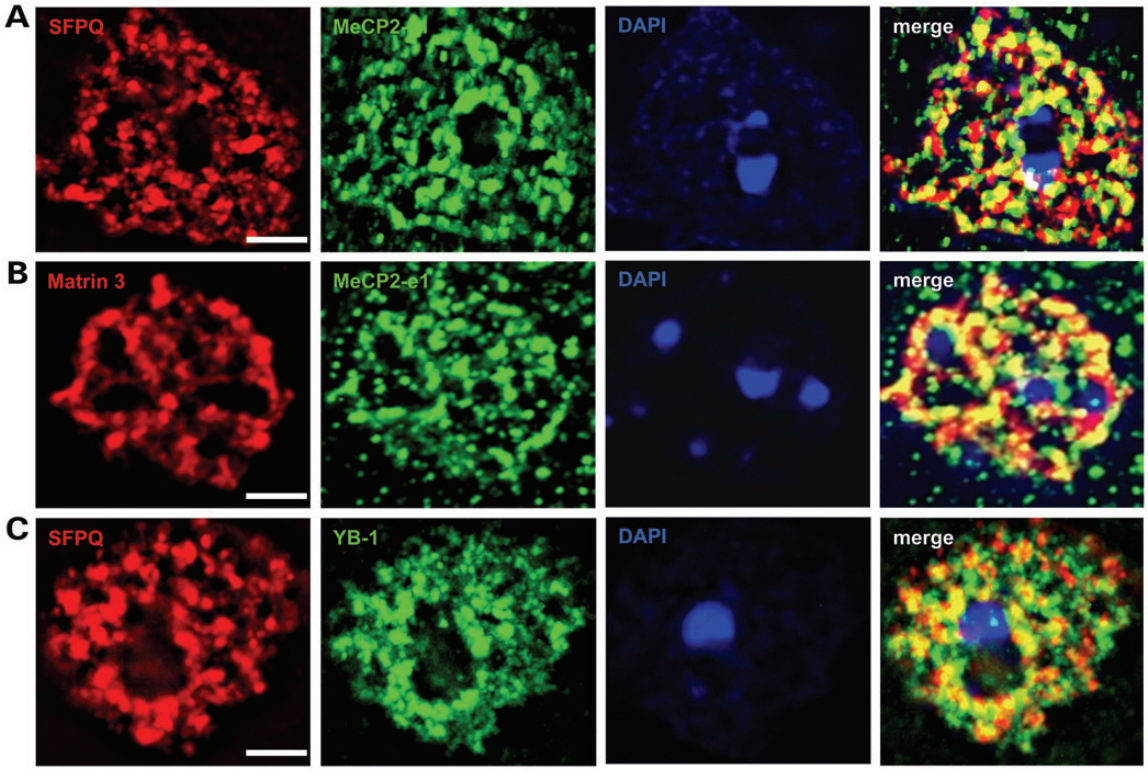

Figure 7. MeCP2-e1 co-localizes with multiple nuclear matrix factors. (**A**) IF staining in cortical neurons for Matrin 3 (red) shows co-localization with MeCP2-e1 (green) distribution as shown by overlapping signal (yellow) in the merge panel. (**B**) Co-staining for SFPQ (red) and MeCP2-e1 (green) similarly shows significant signal overlap (yellow) indicative of co-localization in neuronal nuclei. (**C**). As a positive control, a previously identified MeCP2-associated factor YB-1 (red) also associates with the nuclear matrix as represented by SFPQ signal (green). Overlap of signal distribution is shown in the merged image. In all panels, the location of the nucleus is shown by DAPI counter staining (blue). Scale bars correspond to 5 μm.

mutations (mecp2.chw.edu.au). Therefore, to better recapitulate Rett syndrome in a genetic model system, MeCP2-e1 deficiency was engineered in mice based on an orthologous human mutation (8). MeCP2-e1 was virtually undetectable in the brains of *Mecp2* exon 1 mutant mice rendering them essentially MeCP2-e1 deficient or null (Figs 4 and 5, Supplementary Material, S5, S6, S7 and S10). In terms of RTT, MeCP2-e1 deficient mice exhibited neurologic disease symptoms and died prematurely (Fig. 2). Significantly, MeCP2-e1 deficient mice exhibited abnormal social behaviors and motor defects (Fig. 3) in addition to stereotypies and seizure like symptoms (Supplementary Material, SV1, SV2, SV3). Perhaps most critically, unlike previous RTT mouse models, MeCP2-e1 deficient mice retain MeCP2-e2 expression in brain (Figs 4 and 5, Supplementary Material, S5, S7 and S10) thereby demonstrating that even elevated levels of MeCP2-e2 are not sufficient to prevent the neurological symptoms that result from loss of MeCP2-e1. The results also reveal a novel association of a non-pS30 MeCP2-e1 fraction that localizes to the nucleoplasm and associates with splicing factors that compose the nuclear matrix. Finally, protein stability studies indicate that MeCP2-e1 is more stable than MeCP2-e2 in neurons (Fig. 8). A model of MeCP2-e1 function suggested by these novel findings is shown in Figure 9. Together, these results indicate that MeCP2-e1 has functions distinct from that of MeCP2-e2 in the brain and are consistent with recent studies which showed partial rescue of RTT-like symptoms in *Mecp2* null mice by use of MeCP2-e1 expression constructs (18,31).

However, in seeming contradiction to our results, previous attempts to rescue MeCP2 deficiency by re-expression of MeCP2-e2 alone have been successful in ameliorating survival and at least some neurologic symptoms (18,32,33). In these experiments, MeCP2-e2 was ectopically expressed at levels approaching or exceeding total MeCP2 levels in brain. In the results presented here, brain levels of MeCP2-e2 were elevated in MeCP2-e1 deficient brain compared with WT, but the compensatory increase in MeCP2-e2 levels only restored total brain MeCP2 levels to 50% compared with WT controls. As mentioned, elevated MeCP2-e2 levels were likely due to reduced translation site competition (3). Interestingly, an alternative hypomorphic mouse model expressing 50% of total MeCP2 levels in brain exhibited learning and motor deficits, decreased anxiety and altered social behavior, but not early lethality (34,35). Therefore, the premature lethality observed in MeCP2-e1 deficient mice shown here appears to result from a unique function of MeCP2-e1 that cannot be compensated for by elevated MeCP2-e2 alone.

A potential unique function of MeCP2-e1 is indicated by the unexpected localization results mentioned above. Specifically, IF analysis of WT control mouse brain suggests that at least a sub-fraction of non-pS30 MeCP2-e1 resides in the nucleoplasm *in vivo* (Figs. 4 and 7, Supplementary Material, S4, S5, and S8). In contrast, previous studies with exogenously expressed tagged proteins exhibited a predominant chromocenter localization of both MeCP2-e1 and MeCP2-e2 isoforms (19). However, this

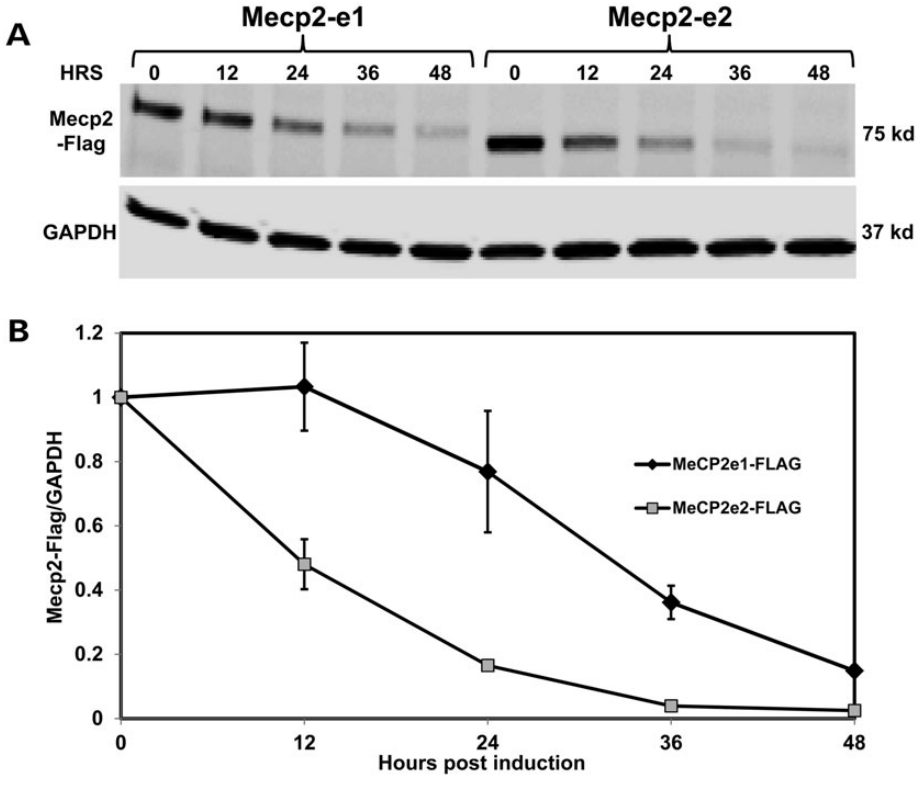

Figure 8. MeCP2-e1 is more stable than MeCP2-e2 in neurons. (**A**) Western blot analysis of flag-tagged MeCP2-e1 and MeCP2-e2 isoform abundance following shutdown of protein expression with doxycycline treatment shown as hours (HRS). Western blot analysis of GAPDH is shown below for normalization. **(B)** The ratio of MeCP2-e1 (black line) and MeCP2-e2 (gray line) compared with GAPDH remaining after expression shutdown is graphed with error bars corresponding to standard error of the mean (SEM).

may be due to ectopic expression levels and/or the influence of the attached tags. In addition, it is possible that exogenously expressed MeCP2 will not be post-translationally modified in the same manner as endogenous MeCP2 isoforms. The unexpected localization of MeCP2-e1 to both chromocenters and nucleoplasm shown above appears to be due to post-translational phosphorylation of serine 30 in amino acid epitopes targeted by MeCP2-e1 antibodies. These results are supported by previous mass spectroscopic analysis (20).

As a follow-up to the MeCP2-e1 localization results, isolation and characterization of non-pS30 MeCP2-e1-associated co-factors identified nuclear matrix factors among other proteins. This suggests that this form of MeCP2-e1 has function in the nucleoplasm where active genes and splicing activity are located on the nuclear matrix (Fig. 9). This function may be related to a critical unique role for MeCP2-e1 in neuronal function and survival. Consistent with these results, previous studies have established the role of MeCP2 in splicing regulation (29,36). While, these studies cannot definitively rule out the possibility that MeCP2-e2 can also associate with the nuclear matrix, the lack of evidence for such association suggests that this is a unique function of MeCP2-e1.

Furthermore, evidence that MeCP2-e1 is more stable than MeCP2-e2 (Fig. 8) suggests that this characteristic may relate to nuclear localization differences and may contribute to the predominant abundance of MeCP2-e1 in brain. Interestingly, *in silico* analysis predicts that MeCP2-e1 is more stable than MeCP2-e2 perhaps due to the addition of an amino terminal acetyl group (http://www.isv.cnrs-gif.fr/terminator3/). In conclusion, investigation of MeCP2-e1 deficient mice demonstrate the relevance of this isoform to RTT pathology and will therefore be important in testing potential therapies designed to alleviate symptoms.

MATERIALS AND METHODS

Ethics statement

All mouse engineering, propagation and analyses protocols were approved by the UC Davis Institutional Animal Care and Use Committee (IACUC) and Biological Use Authority (BUA) protocols. These protocols conform to current National Institutes of Health (NIH) and the American Association of Lab Animal Standards (AALAS) regulatory standards.

Transgenic mouse generation

Mecp2-e1 transgenic mice were engineered by the UC Davis Mouse Biology Program. Briefly, site directed mutagenesis was used to alter the *exon 1* translational start site ATG to TTG in the *Mecp2* locus excised from a genomic bacterial artificial chromosome (BAC) clone. A neomycin resistance gene (NEO) flanked by Flippase recognition target sites (FRT) was inserted into the first intron to produce the targeting vector (top) which was then electroporated in C57BL/6N ES cells for homologous recombination. ES cells incorporating the targeting

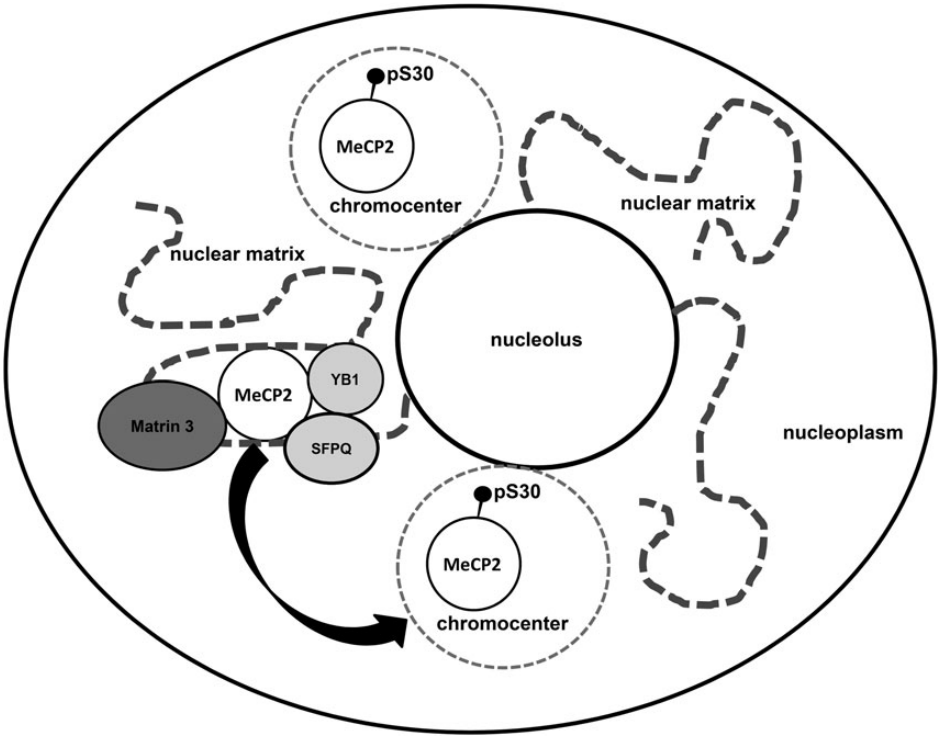

Figure 9. A model of MeCP2-e1 function in neurons. In this model, non-pS30 MeCP2-e1 forms a molecular complex with RNA regulatory factors on the nuclear matrix in the neuronal nucleoplasm. Neuronal signals trigger phosphorylation of MeCP2 at phosphoserine 30 leading to dissociation from the nuclear matrix and relocalization of MeCP2 to heterochromatin in chromocenters.

vector were selected for growth in the presence of neomycin prior to expression of Flippase recombination enzyme for removal of the NEO cassette thus generating the *Mecp2* mutant allele (Supplementary Material, Fig. S1). ES clones selected by karyotype were microinjected into Balb/C embryos, 31 of which were implanted into two pseudo-pregnant Balb/C female mice that produced 16 chimeric pups. Two chimeric males with >95% black coat color were selected as founders and mated with C57BL/6N females to produce *Mecp2 exon 1*+/− heterozygous females which were mated with C57BL/6N males to produce the four possible genotypes of *Mecp2 exon 1* transgenic mice, −/y, +/y, −/+ and +/+. Genotyping was performed by PCR using primers against the WT *Mecp2* and transgenic alleles (Fig. 1).

IP and mass spectrometric protein identification

Nuclear extracts from SH-SY5Y neurons differentiated by 48 h treatment with PMA were prepared according to Dignam (37) and immuno-precipitated with chicken anti-MeCP2-e1 JL (Aves Labs, Tigard, OR, USA) and control antibodies. MeCP2-e1 associated proteins were bound to precipHen agarose beads (Aves Labs), washed extensively, denatured and resolved by 4–15% SDS–PAGE. Resolved proteins were stained in the gel with GelCode Blue (Thermo Scientific, Rockford, IL, USA), then digested in gel with trypsin. Digested peptides were then separated by liquid chromatography and subject to tandem mass spectrometric–mass spectrometric (MS–MS) analysis on an LTQ Mass spectrometer (Thermo Scientific) to determine peptide sequences. Mascot MS–MS ion search was then used to analyze raw MS–MS data (www.matrixscience.com). Only peptides with ion scores of >46 were used for Mascot sequence query to assign peptides to proteins. Ions scores are $-10\log(P)$, where P is the probability that the observed match is a random event and ions scores of >46 indicate identity or homology ($P < 0.05$) (www.matrixscience.com).

Co-IP and western analysis

Antibodies to MeCP2-e1 (Aves Labs), Matrin 3 (Bethyl, Montgomery, TX, USA) and SFPQ (Abcam, Cambridge, MA, USA) were incubated with SH-SY5Y nuclear proteins. Antibody/protein complexes were recovered by binding to protein A/G beads, washed extensively, resolved by SDS–PAGE then transferred to nylon membranes. Western blots were then probed with primary antibodies which were detected by a combination of HRP conjugated secondary antibodies and West Dura chemiluminescent substrate (Pierce, Rockford, IL, USA). Chemiluminescent signals were detected and quantified using a Fluorchem Imager (Alpha Innotech, San Leandro, CA, USA).

Western analysis

Brains were removed from *Mecp2-e1*$^{-/y}$ deficient and *Mecp2-e1*$^{+/y}$ control mice, dounce homogenized in 1× PBS buffer containing 2% SDS supplemented with protease inhibitors (Roche, Indianapolis, IN, USA). Soluble brain proteins were resolved by SDS–PAGE, transferred to nylon membranes

and probed with antibodies to MeCP2-e1 CS (custom), and MeCP2-e2 (Thermo Scientific) and Gapdh (Advanced, Long Beach, CA, USA). Lymphoblastoid cell lines were generated from peripheral blood of RTT patients as described previously (8,13). For western analysis of MeCP2-e1, lymphoblastoid cells were propagated in culture, lysed in 2% SDS sample buffer and resolved by gel electrophoresis before transfer to nylon membranes and probing with MeCP2-e1 JL and MeCP2-e1 CS antibodies.

Immunofluorescence

Brains were removed from mice then divided by cutting along the medial longitudinal fissure. The left hemisphere was fixed in 4% formaldehyde/1× PBS for 72 h, washed in 1× PBS then dehydrated in 70% ethanol. Fixed brains were embedded in paraffin and sectioned into 5 μM coronal slices and affixed to glass slides. Brain sections were de-paraffinized then heated in citrate buffer to recover epitopes followed by probing with MeCP2 primary and fluorescently labeled secondary antibodies (Thermo/Fisher, Rockford, IL). Images were captured using a CCD camera (Qimaging, Surrey, BC, Canada) on an Axioplan 2 microscope (Carl Zeiss, Thornwood, NY, USA) and analyzed using iVision software (Scanalytics, Vienna, VA, USA). MeCP2-e1 MR and MeCP2-e1 antibodies were obtained through collaborative agreement while MeCP2-e2-specific antibody was purchased from Pierce (Thermo/Pierce, Rockford, IL).

Mouse phenotyping

A scoring system loosely based on Guy *et al*. (9,38) was devised for ranking mice according to disease severity. Mice were evaluated in a blinded manner at weekly intervals from 3 weeks of age (weaning) for matted fur, reduced ambulation, open skin sores and an abnormally large abdomen along with specific responses to tail suspension including hindlimb clasping, forelimb 'washing' and the absence of flailing motions. A point was assigned for each characteristic thus scores of severely affected mice would approach '7' while control littermate scores approach '0'. According to UC Davis IACUC policy, mice that are unable to ingest food and water or have open, non-healing skin lesions must be euthanized to minimize suffering. Hence, some of the MeCP2-e1 deficient mice did not die unassisted.

Body weights and lengths were measured at the beginning of the testing and body weights were measured at the conclusion of the 1-week test period. Tests were scheduled 2–3 days apart to minimize stress. There were no significant differences in initial weight, final weight, weight change, body length or body mass index (weight/length). The mice were also screened for condition, cataracts, whisker barbering, gait and tail hang. We selected the test cohort at an age prior to the onset of neurologic and morbidity symptoms.

Elevated plus maze

Mice were analyzed as described in Woods *et al*. (39). Briefly, test mice were placed onto the central platform of the plus maze without acclimation and allowed 5 min of free exploration in the apparatus. Mouse behavior was recorded under dim red light by video camera (Sony Digital Handycam) and analyzed using the SMART tracking system (San Diego Instrument, San Diego, CA, USA). Distance traveled, number of entries and duration of time spent in the open versus closed arms were recorded.

Sociability

The sociability preference test was performed using a three-chamber assay as established in previous studies (39,40). Briefly, a test animal was placed in the center compartment (zone) and allowed to explore and acclimate to the test environment for 10 min. An object mouse was then placed in one of the cages and the test animal was again released in the center compartment and videotaped for a total of 10 min with the object mouse. Topscan (Clever Systems, Reston, VA, USA) software was used to determine location of the test mouse in each chamber and in proximity to each cage.

Ambulation (gait)

Mice were subject to TreadScan analysis as described previously (41). For TreadScan trials mice were placed on a moving tread mill and video recorded from below through a clear window. Automated video analysis using foot placement software (Clever Systems, Reston, VA, USA) was then performed. Mice were assessed by their stride length, foot splay, running speed and trajectory of foot stance for indications of abnormal ambulation

Statistical analysis

For western blot analysis and disease scoring, two-sample *t*-tests were performed with each genotype representing independent samples for the two-tailed test assuming unequal sample variances using Vasserstats.net. For mouse behavioral comparisons, least square ANOVA (JMP, Version 10, SAS Institute, Cary, NC, USA) was used with genotype as the independent variable and covariates when appropriate. Statistical significance was indicated at $P < 0.05$ by*.

MeCP2 isoform stability analysis

Previously described *Mecp2-e1* and *Mecp2-e2* Flag expression vectors (20) were engineered with a 5′ tetracycline transcriptional transactivator response element (TRE) using a Tet-off Advanced system (Clontech, Mountain View, CA, USA). SH-SY5Y cells stably expressing the Tet-off Advanced transactivator (Clontech) were transiently transfected with the pTRE MeCP2-Flag vectors. Addition of tetracycline or doxycycline prevents binding of the transcriptional transactivator to the *Mecp2* constructs and expression of MeCP2-e1 or MeCP2-e2 Flag protein can be shut off in the transfected cells. Flag-tagged MeCP2-e1 and MeCP2-e2 protein levels were assessed from whole cell lysates, 12, 24, 36 and 48 h after doxycycline treatment by western blot using a LiCor Odyssey quantitative imaging system.

SUPPLEMENTARY MATERIAL

Supplementary Material is available at *HMG* online.

AUTHORS' CONTRIBUTIONS

D.H.Y. conceived and designed experiments, performed experiments, analyzed data and wrote the manuscript. N.C.S., M.R. and C.O.O. provided antibodies, contributed technical advice and edited the manuscript. J.B.V. contributed RTT cell lines and consulted on experimental approach. J.O.A. and D.J.H. performed experiments. M.L.G. designed and performed experiments and consulted on experimental approach. B.J.G. designed and engineered transgenic mice. F.K.C. performed experiments and assisted with mouse colony management. M.S.G. performed mouse behavioral data analysis and assisted with experimental design. J.M.L. consulted on experimental design and edited the manuscript.

ACKNOWLEDGEMENTS

We acknowledge the UC Davis Mouse Biology Program (MBP) for transgenic mouse generation services. Sasha S. Wirth coordinated these efforts. The Mouse Behavioral Assessment Lab (MBAL) division of MBP managed by Peter T. Takeuchi also performed invaluable mouse phenotyping and behavioral analysis services.

Conflict of Interest statement. None declared.

FUNDING

This work was supported by Grants 2R01HD041462 to J.M.L. and 1R01NS081913 to J.M.L. from the National Institutes of Health (NIH) and Grants #2911 to D.H.Y. and #2542 to D.H.Y.) from the International Rett Syndrome Foundation (IRSF).

REFERENCES

1. Amir, R.E., Van den Veyver, I.B., Wan, M., Tran, C.Q., Francke, U. and Zoghbi, H.Y. (1999) Rett syndrome is caused by mutations in X-linked MECP2, encoding methyl-CpG-binding protein 2. *Nat. Genet.*, **23**, 185–188.
2. Coy, J.F., Sedlacek, Z., Bachner, D., Delius, H. and Poustka, A. (1999) A complex pattern of evolutionary conservation and alternative polyadenylation within the long 3′-untranslated region of the methyl-CpG-binding protein 2 gene (MeCP2) suggests a regulatory role in gene expression. *Hum. Mol. Genet.*, **8**, 1253–1262.
3. Kriaucionis, S. and Bird, A. (2004) The major form of MeCP2 has a novel N-terminus generated by alternative splicing. *Nucleic Acids Res.*, **32**, 1818–1823.
4. Mnatzakanian, G.N., Lohi, H., Munteanu, I., Alfred, S.E., Yamada, T., MacLeod, P.J., Jones, J.R., Scherer, S.W., Schanen, N.C., Friez, M.J. *et al.* (2004) A previously unidentified MECP2 open reading frame defines a new protein isoform relevant to Rett syndrome. *Nat. Genet.*, **36**, 339–341.
5. Zachariah, R.M., Olson, C.O., Ezeonwuka, C. and Rastegar, M. (2012) Novel MeCP2 isoform-specific antibody reveals the endogenous MeCP2E1 expression in murine brain, primary neurons and astrocytes. *PloS ONE*, **7**, e49763.
6. Amir, R.E., Fang, P., Yu, Z., Glaze, D.G., Percy, A.K., Zoghbi, H.Y., Roa, B.B. and Van den Veyver, I.B. (2005) Mutations in exon 1 of MECP2 are a rare cause of Rett syndrome. *J. Med. Genet.*, **42**, e15.
7. Quenard, A., Yilmaz, S., Fontaine, H., Bienvenu, T., Moncla, A., des Portes, V., Rivier, F., Mathieu, M., Raux, G., Jonveaux, P. *et al.* (2006) Deleterious mutations in exon 1 of MECP2 in Rett syndrome. *Eur. J. Med. Genet.*, **49**, 313–322.
8. Saunders, C.J., Minassian, B.E., Chow, E.W., Zhao, W. and Vincent, J.B. (2009) Novel exon 1 mutations in MECP2 implicate isoform MeCP2_e1 in classical Rett syndrome. *Am. J. Med. Genet A.*, **149A**, 1019–1023.
9. Guy, J., Hendrich, B., Holmes, M., Martin, J.E. and Bird, A. (2001) A mouse Mecp2-null mutation causes neurological symptoms that mimic Rett syndrome. *Nat. Genet.*, **27**, 322–326.
10. Chen, R.Z., Akbarian, S., Tudor, M. and Jaenisch, R. (2001) Deficiency of methyl-CpG binding protein-2 in CNS neurons results in a Rett-like phenotype in mice. *Nat. Genet.*, **27**, 327–331.
11. Pelka, G.J., Watson, C.M., Radziewic, T., Hayward, M., Lahooti, H., Christodoulou, J. and Tam, P.P. (2006) Mecp2 deficiency is associated with learning and cognitive deficits and altered gene activity in the hippocampal region of mice. *Brain*, **129**, 887–898.
12. Itoh, M., Tahimic, C.G., Ide, S., Otsuki, A., Sasaoka, T., Noguchi, S., Oshimura, M., Goto, Y. and Kurimasa, A. (2012) Methyl CpG-binding protein isoform MeCP2-e2 is dispensable for Rett syndrome phenotypes but essential for embryo viability and placenta development. *J. Biol. Chem.*, **287**, 13859–13867.
13. Gianakopoulos, P.J., Zhang, Y., Pencea, N., Orlic-Milacic, M., Mittal, K., Windpassinger, C., White, S.J., Kroisel, P.M., Chow, E.W., Saunders, C.J. *et al.* (2012) Mutations in MECP2 exon 1 in classical Rett patients disrupt MECP2_e1 transcription, but not transcription of MECP2_e2. *Am. J. Med. Genet. B Neuropsychiatr. Genet.*, **159B**, 210–216.
14. Shahbazian, M., Young, J., Yuva-Paylor, L., Spencer, C., Antalffy, B., Noebels, J., Armstrong, D., Paylor, R. and Zoghbi, H. (2002) Mice with truncated MeCP2 recapitulate many Rett syndrome features and display hyperacetylation of histone H3. *Neuron*, **35**, 243–254.
15. Goffin, D., Allen, M., Zhang, L., Amorim, M., Wang, I.T., Reyes, A.R., Mercado-Berton, A., Ong, C., Cohen, S., Hu, L. *et al.* (2011) Rett syndrome mutation MeCP2 T158A disrupts DNA binding, protein stability and ERP responses. *Nat. Neurosci.*, **15**, 274–283.
16. Chahrour, M. and Zoghbi, H.Y. (2007) The story of Rett syndrome: from clinic to neurobiology. *Neuron*, **56**, 422–437.
17. Rastegar, M., Hotta, A., Pasceri, P., Makarem, M., Cheung, A.Y., Elliott, S., Park, K.J., Adachi, M., Jones, F.S., Clarke, I.D. *et al.* (2009) MECP2 isoform-specific vectors with regulated expression for Rett syndrome gene therapy. *PloS ONE*, **4**, e6810.
18. Kerr, B., Soto, C.J., Saez, M., Abrams, A., Walz, K. and Young, J.I. (2012) Transgenic complementation of MeCP2 deficiency: phenotypic rescue of Mecp2-null mice by isoform-specific transgenes. *Eur. J. Hum. Genet.*, **20**, 69–76.
19. Kumar, A., Kamboj, S., Malone, B.M., Kudo, S., Twiss, J.L., Czymmek, K.J., LaSalle, J.M. and Schanen, N.C. (2008) Analysis of protein domains and Rett syndrome mutations indicate that multiple regions influence chromatin-binding dynamics of the chromatin-associated protein MECP2 in vivo. *J. Cell Sci.*, **121**, 1128–1137.
20. Gonzales, M.L., Adams, S., Dunaway, K.W. and LaSalle, J.M. (2012) Phosphorylation of distinct sites in MeCP2 modifies cofactor associations and the dynamics of transcriptional regulation. *Mol. Cell. Biol.*, **32**, 2894–2903.
21. Nan, X., Campoy, F.J. and Bird, A. (1997) MeCP2 is a transcriptional repressor with abundant binding sites in genomic chromatin. *Cell*, **88**, 471–481.
22. Brero, A., Easwaran, H.P., Nowak, D., Grunewald, I., Cremer, T., Leonhardt, H. and Cardoso, M.C. (2005) Methyl CpG-binding proteins induce large-scale chromatin reorganization during terminal differentiation. *J. Cell. Biol.*, **169**, 733–743.
23. Salton, M., Lerenthal, Y., Wang, S.Y., Chen, D.J. and Shiloh, Y. (2010) Involvement of Matrin 3 and SFPQ/NONO in the DNA damage response. *Cell Cycle*, **9**, 1568–1576.
24. Malyavantham, K.S., Bhattacharya, S., Barbeitos, M., Mukherjee, L., Xu, J., Fackelmayer, F.O. and Berezney, R. (2008) Identifying functional neighborhoods within the cell nucleus: proximity analysis of early S-phase replicating chromatin domains to sites of transcription, RNA polymerase II, HP1gamma, matrin 3 and SAF-A. *J. Cell. Biochem.*, **105**, 391–403.
25. Berezney, R., Mortillaro, M.J., Ma, H., Wei, X. and Samarabandu, J. (1995) The nuclear matrix: a structural milieu for genomic function. *Int. Rev. Cytol.*, **162A**, 1–65.

26. Small, D., Nelkin, B. and Vogelstein, B. (1982) Nonrandom distribution of repeated DNA sequences with respect to supercoiled loops and the nuclear matrix. *Proc. Natl. Acad. Sci. USA*, **79**, 5911–5915.
27. Malyavantham, K.S., Bhattacharya, S., Alonso, W.D., Acharya, R. and Berezney, R. (2008) Spatio-temporal dynamics of replication and transcription sites in the mammalian cell nucleus. *Chromosoma*, **117**, 553–567.
28. Yasui, D., Miyano, M., Cai, S., Varga-Weisz, P. and Kohwi-Shigematsu, T. (2002) SATB1 targets chromatin remodelling to regulate genes over long distances. *Nature*, **419**, 641–645.
29. Young, J.I., Hong, E.P., Castle, J.C., Crespo-Barreto, J., Bowman, A.B., Rose, M.F., Kang, D., Richman, R., Johnson, J.M., Berget, S. *et al.* (2005) Regulation of RNA splicing by the methylation-dependent transcriptional repressor methyl-CpG binding protein 2. *Proc. Natl. Acad. Sci. USA*, **102**, 17551–17558.
30. Chandler, S.P., Guschin, D., Landsberger, N. and Wolffe, A.P. (1999) The methyl-CpG binding transcriptional repressor MeCP2 stably associates with nucleosomal DNA. *Biochemistry*, **38**, 7008–7018.
31. Gadalla, K.K., Bailey, M.E., Spike, R.C., Ross, P.D., Woodard, K.T., Kalburgi, S.N., Bachaboina, L., Deng, J.V., West, A.E., Samulski, R.J. *et al.* (2013) Improved survival and reduced phenotypic severity following AAV9/MECP2 gene transfer to neonatal and juvenile male Mecp2 knockout mice. *Mol. Ther.*, **21**, 18–30.
32. Luikenhuis, S., Giacometti, E., Beard, C.F. and Jaenisch, R. (2004) Expression of MeCP2 in postmitotic neurons rescues Rett syndrome in mice. *Proc. Natl. Acad. Sci. USA*, **101**, 6033–6038.
33. Giacometti, E., Luikenhuis, S., Beard, C. and Jaenisch, R. (2007) Partial rescue of MeCP2 deficiency by postnatal activation of MeCP2. *Proc. Natl. Acad. Sci. USA*, **104**, 1931–1936.
34. Samaco, R.C., Fryer, J.D., Ren, J., Fyffe, S., Chao, H.T., Sun, Y., Greer, J.J., Zoghbi, H.Y. and Neul, J.L. (2008) A partial loss of function allele of methyl-CpG-binding protein 2 predicts a human neurodevelopmental syndrome. *Hum. Mol. Genet.*, **17**, 1718–1727.
35. Kerr, B., Alvarez-Saavedra, M., Saez, M.A., Saona, A. and Young, J.I. (2008) Defective body-weight regulation, motor control and abnormal social interactions in Mecp2 hypomorphic mice. *Hum. Mol. Genet.*, **17**, 1707–1717.
36. Maunakea, A.K., Chepelev, I., Cui, K. and Zhao, K. (2013) Intragenic DNA methylation modulates alternative splicing by recruiting MeCP2 to promote exon recognition. *Cell Res.*, **23**, 1256–1269.
37. Dignam, J.D., Lebovitz, R.M. and Roeder, R.G. (1983) Accurate transcription initiation by RNA polymerase II in a soluble extract from isolated mammalian nuclei. *Nucleic Acids Res.*, **11**, 1475–1489.
38. Guy, J., Gan, J., Selfridge, J., Cobb, S. and Bird, A. (2007) Reversal of neurological defects in a mouse model of Rett syndrome. *Science*, **315**, 1143–1147.
39. Woods, R., Vallero, R.O., Golub, M.S., Suarez, J.K., Ta, T.A., Yasui, D.H., Chi, L.H., Kostyniak, P.J., Pessah, I.N., Berman, R.F. *et al.* (2012) Long-lived epigenetic interactions between perinatal PBDE exposure and Mecp2308 mutation. *Hum. Mol. Genet.*, **21**, 2399–2411.
40. Moy, S.S., Nadler, J.J., Perez, A., Barbaro, R.P., Johns, J.M., Magnuson, T.R., Piven, J. and Crawley, J.N. (2004) Sociability and preference for social novelty in five inbred strains: an approach to assess autistic-like behavior in mice. *Genes Brain Behav.*, **3**, 287–302.
41. Golub, M.S., Germann, S.L., Araiza, R.S., Reader, J.R., Griffey, S.M. and Lloyd, K.C. (2005) Movement disorders in the Hfe knockout mouse. *Nutr. Neurosci.*, **8**, 239–244.